Eleventh International Conference on CFD in the Minerals and Process Industries
CSIRO, Melbourne, Australia
7-9 December 2015

A MULTIPHASE GRAY-SCALE LATTICE BOLTZMANN MODEL

Gerald G. PEREIRA*

CSIRO Digital Productivity Flagship, Clayton, Victoria 3169, AUSTRALIA
*Corresponding author, E-mail address: Gerald.Pereira@csiro.au

ABSTRACT

The Lattice Boltzmann (LB) method has been shown to be a highly efficient numerical method for solving fluid flow in confined domains such as pipes, irregularly shaped channels or porous media. Traditionally the LB method has been applied to flow in void regions (pores) and no flow in solid regions. However, in a number of scenarios, this may not suffice. That is partial flow may occur in semi-porous regions. Recently gray-scale LB methods have been applied to model single phase flow in such semi-porous materials. Voxels are no longer completely void or completely solid but somewhere in between. We extend the LB method to model multiphase flow (e.g., gas and liquid or water and oil) in a semi-porous medium. We compare the solution to test cases as well as applying it to real porous media.

NOMENCLATURE

n_s fluid bounce-back fraction
f LB distribution function, [dimensionless].
P LB pressure, [dimensionless].
$\boldsymbol{r}$ LB lattice position, [dimensionless].
$\boldsymbol{u}$ LB velocity, [dimensionless].
$\boldsymbol{e}$ LB discrete velocity vectors, [dimensionless].
F LB force, [dimensionless].
g LB interaction between phases [dimensionless].
c_s LB speed of sound, [dimensionless].
w LB weights, [dimensionless].

ρ LB particle density [dimensionless]
v LB kinematic viscosity [dimensionless]

Sub/superscripts
k multiphase component.
i LB velocity direction.

INTRODUCTION

The Lattice Boltzmann method (LBM) has been developed over the past thirty years and has proven to be a numerically efficient and accurate method to model fluid flow in confined, topologically complex geometrical domains. LBM does not directly solve the Navier-Stokes equations but rather the Boltzmann transport equation. Through a Chapman-Enskog expansion it can be shown the solution obtained with LBM is equivalent to that which would have been obtained from a direct solve of the Navier-Stokes equation (Succi, 2001). LBM is now commonly applied to determine the permeability of complex porous media such as carbonate rocks, shales and so on (e.g., Liu et al, 2014). The inputs for these computations are a digital representation of the porous medium which usually comes from CT scans. Here each voxel corresponds to a solid region (not available for fluid flow) or void region (available for fluid flow). Suitable boundary conditions are applied at boundaries between solid and void voxels, to account for a no-slip boundary condition. Steady state fluid flows can then be obtained iteratively and from this the medium's permeability. We refer to such a model as a black-white (BW) model.

The typical resolution of CT scans is of the order of 1-10 microns. However, in many mineral rocks, the grain size is much smaller than this – maybe of the order of 10-100 nanometres or so. This means a given voxel will contain both solid and pore regions. Moreover, rocks are constituted of more than one material and these materials can have different slip conditions, which will affect resistance to fluid flow. This discussion implies a BW model will not be adequate for a range of rocks which are or current interest to those in the petroleum and natural gas industries. Rather a model which allows for differing amounts of flow depending on that voxel's (fractional) solid constitution is required. This has been the motivation behind the development of so called "*gray-scale*" LBM models (Balasubramanian et al, 1987, Gao and Sharma, 1994, Dardis and McCloskey, 1998).

LBM is a class of *cellular automata* which is solved on a regular lattice (usually simple-cubic in 3D). On each lattice vertex/node a set of fluid particle distribution functions is defined. There are Q distribution functions defined on each node. LBM then consists of three main steps. The first step is called *streaming* in which all fluid packets (distributions) are moved to adjacent sites. This streaming can be correlated to the normal advection of fluid. The second step is called *bounce-back* which accounts for fluid-solid boundary conditions. Here fluid packets at boundary nodes are reversed in direction (actually a more complicated rule is used, but essentially this is the result). The final step in LBM is a *collision* step where fluid packets converging on a given node are re-distributed according to a given rule. The LBM method then consists of iterating these three steps to give a solution. This procedure works well for a BW model. In the gray-scale models there are no fluid-solid boundaries, as such. All voxels are allowed a certain degree of flow. This can be related to the solid fraction in that voxel, but other effects such as tortuosity, topology, mineral content etc can be included into the model to contribute to the voxel's resistance to flow. To account for a voxel's resistance to flow, we now impose a partial bounce-back rule on each voxel. This means at each voxel, a certain fraction of fluid packets (which were streamed into a node) will be bounced back. We denote the fraction of

fluid packets which are bounced back at a node by n_s, where $0 \leq n_s \leq 1$ and each node can have a different n_s.

The gray-scale model just described has now been implemented to simulate single phase fluid flow in real rocks, which are made up of a number of different minerals (Li et al, 2014a). The mineral content for each voxel was extracted using a DCM methodology (see https://en.wikipedia.org/wiki/Data_constrained_modelling) and then these fractional contents were used in combination with a simple rule to give an n_s value for each voxel. Not only were the results numerically stable but they were also physically realistic which makes this method a suitable candidate for future studies. It is noted here this method can also be used to upscale permeability to larger sample sizes, as long as an effective fluid resistance can be obtained for individual elements.

Multiphase fluid flow (e.g. oil and water or gas and oil) is of utmost importance in the petroleum industry. Two or three phase relative permeabilities are notoriously difficult to obtain experimentally. A numerical method which can calculate these permeabilities will be of significant benefit. With this in mind we now consider applying the gray-scale model to multiphase fluid flow. Multiphase LB models have already been developed. A previous publication of ours (Pereira, 2015) briefly reviews these methods as well as outlining the multiphase LB method we shall use (*pseudo-potential* LBM model). Thus in the remainder of this paper we briefly describe the multiphase gray-scale LBM model. We compare it with some test cases as well as applying it to sample porous media.

LB MODEL

Single phase gray-scale LB model

The LB model is a mesoscopic numerical method used to study incompressible fluid dynamics. Its main advantages over more conventional CFD techniques (which directly solve the Navier-Stokes equations) are its programming simplicity, computational efficiency and inherent parallelism due to a large amount of local computations. In addition, as mentioned in the Introduction, it naturally deals with complex porous media if suitable digital information is provided. Details of this method, applied to single phase flow, are available (Succi, 2001; Chen and Doolen, 1998) and thus we shall only focus here on the LB method applied to gray-scale models.

As explained in the Introduction, LB consists of streaming, collision and bounce-back at boundaries. More complex and accurate boundary conditions such as half-way bounce-back or linear interpolation boundary conditions are also possible. In the collision step particle distributions relax towards a given equilibrium distribution - a Maxwellian distribution. Then macroscopic properties such as fluid density, fluid velocity and the stress tensor can be derived from the particle distributions. If we are dealing with only a single fluid, one set of particle distributions is defined, i.e. $f(\boldsymbol{r}, \boldsymbol{u}, t)$ which denotes the distribution of particles travelling with a particular velocity $\boldsymbol{u}$ at time t at lattice node $\boldsymbol{r}$. We will only consider a three dimensional (3D) model in this paper so that we implement the common D3Q19 model which indicates that there are 18 possible vectors, $\boldsymbol{e}_i$, in which particles may move in addition to the null vector. These 18 possibilities are the vectors $(\pm1, 0, 0)$, $(0,\pm1,0)$, $(0,0,\pm1)$, $(\pm1,\pm1,0)$, $(\pm1,0,\pm1)$, $(0,\pm1,\pm1)$.
We solve the following LB equation at every node for the distribution function with velocity e_i:

$$\mathrm{f_i}(\boldsymbol{r}+\boldsymbol{e}_\mathrm{i}\Delta\mathrm{t},\mathrm{t}+\Delta\mathrm{t})-\mathrm{f_i}(\boldsymbol{r},\mathrm{t})=-\frac{1}{\tau}\left[\mathrm{f_i}(\boldsymbol{r},\mathrm{t})-\mathrm{f_i^{eq}}(\boldsymbol{r},\mathrm{t})\right]. \quad (1)$$

The term f_i^{eq} is the equilibrium Maxwell distribution given by

$$\mathrm{f_i}=\mathrm{w_i}\rho\left[1+\frac{\boldsymbol{e}_\mathrm{i}\bullet\boldsymbol{u}^{eq}}{\mathrm{c_s^2}}+\frac{(\boldsymbol{e}_\mathrm{i}\bullet\boldsymbol{u}^{eq})^2}{2\mathrm{c_s^4}}-\frac{\boldsymbol{u}^{eq}\bullet\boldsymbol{u}^{eq}}{2\mathrm{c_s^2}}\right], \quad (2)$$

where w_i are weights which are defined for the given D3Q19 model. In Eq.(1), τ represents a relaxation time and it can be shown to be related to kinematic viscosity via $\nu = c_s^2(\tau - 1/2)$ where c_s is the sound speed and c_s^2 equals 1/3. The pressure, p, in this model is given by the equation of state $P = c_s^2\rho$. The LB equation (1) is known in the literature as single relaxation time (SRT) scheme, because only one relaxation time is involved.

The relationship to macroscopic parameters such as density and velocity are given by

$$\rho=\sum_\mathrm{i}\mathrm{f_i} \quad \textit{and} \quad \rho\boldsymbol{u}=\sum_\mathrm{i}\mathrm{f_i}\boldsymbol{e}_\mathrm{i}. \quad (3)$$

To model forces (such as body forces to mimic gravity or even surface forces between different phases when we model two or more phases) we add an explicit forcing term to the LB equation (1). This forcing term is defined by He *et al* (1998)

$$\Im_i=\frac{\mathrm{F}\bullet(\boldsymbol{e}_\mathrm{i}-\boldsymbol{u}^{\mathrm{eq}})}{\rho\mathrm{c_s^2}}\mathrm{f_i^{eq}}, \quad (4)$$

where $\boldsymbol{F}$ is the force. The macroscopic velocities are modified in this case to $\rho\boldsymbol{u}=\sum_\mathrm{i}\mathrm{f_i}\boldsymbol{e}_\mathrm{i}+\boldsymbol{F}/2$ and $\boldsymbol{u}^{eq}=\boldsymbol{u}$.

This implementation of an applied force is not only accurate, but also exhibits correct time evolution of the flow.

Typically LB methods solve on (100%) void nodes and don't solve on solid nodes. To simulate no-slip boundary conditions, at boundaries between void and solid nodes, a bounce-back step is performed which simply reverses the direction of the streamed distribution function. In the gray LB methods, one solves at *all* nodes. Since there are no solid nodes, as such, a full bounce back is not performed. Rather, on any given node a certain fraction of the fluid packets that are streamed into that node are bounced back. This fraction of fluid packets which are bounced back at any given node is given by n_s and so equation (1) is replaced by

$$\mathrm{f_i}(\boldsymbol{r}+\boldsymbol{e}_\mathrm{i}\Delta\mathrm{t},\mathrm{t}+\Delta\mathrm{t})=(1-n_s)\mathrm{f_i}(\boldsymbol{r},\mathrm{t})-\frac{1}{\tau}(1-n_s)\left[\mathrm{f_i}(\boldsymbol{r},\mathrm{t})-\mathrm{f_i^{eq}}(\boldsymbol{r},\mathrm{t})\right]+(1-n_s)\Im_i+n_s\,\widehat{\mathrm{f_i}}(\boldsymbol{r},\mathrm{t}). \quad (5)$$

The last term with the circumflex on the distribution function indicates the distribution function to be added is in the opposite direction to i. The parameter n_s is between 0 and 1, and can be related to voxel compositional and/or topological properties (among other things). The macroscopic velocity is now

$$\rho\boldsymbol{u}=(1-n_s)\left(\sum_\mathrm{i}\mathrm{f_i}\boldsymbol{e}_\mathrm{i}+\boldsymbol{F}/2\right). \quad (6)$$

Equation 5 represents the gray-scale LB model (Walsh et al, 2009) and has been validated both for test cases such as the Brinkman equation and on real samples (Li et al, 2014) with good accuracy. For example, in Fig. 1 we show comparisons between the analytic solution of the Darcy-Brinkman equation and LB simulations. The Darcy-Brinkman equation models laminar flow through a channel which has a non-zero resistance (or drag). It is given by

$$\nabla^2 u - \left(\frac{\varphi}{\nu_B}\right) u = \frac{1}{\rho \nu_B} G \quad , \qquad (7)$$

where φ is the resistance to flow in some local region, ν_B is the Brinkman viscosity and G is the body force. The solution of this equation is

$$u(y) = -\frac{G}{\varphi\rho}\left[1 - \frac{\cosh[r(y - H/2)]}{\cosh(r \cdot H/2)}\right] \quad , \quad (8)$$

where $r = \sqrt{\varphi/\nu}_B$ and $\varphi = 2n_s$. Figure 1 shows a good overall correlation between LB simulations and Eq. (8) for various n_s values. There is a bit of discrepancy near the walls (at H=1 and H=51) for the larger n_s values. A detailed resolution study and its effects on limiting the error between the analytic and LB solution is beyond the scope of this work, but will be carried out and reported in a future publication.

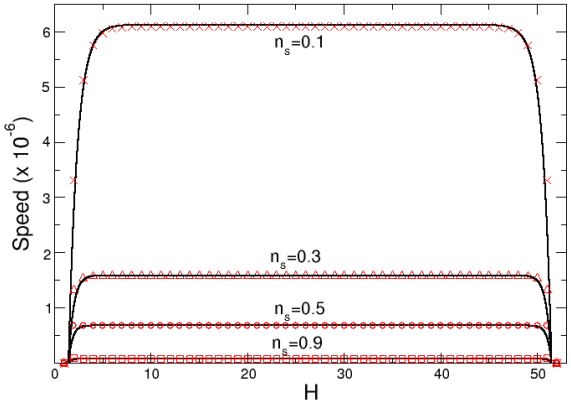

Figure 1: Comparison between Brinkman flow analytic solution for single phase flow and LB gray-scale model. Curves are analytic solutions and symbols are LB results for various n_s values with G = 1.36x10^{-6}.

Multi-phase gray-scale LB model

Figure 1 gives us some confidence in the single phase gray-scale LB model so that we now proceed to applying an extension of it to two (or more) immiscible phases. In principle there can be n phases. To model this with our LB method we now define n sets of distributions functions, which represent each immiscible phase - $f^1(\boldsymbol{r},\boldsymbol{u},t)$ ... $f^n(\boldsymbol{r},\boldsymbol{u},t)$. For each phase we solve the LB equation at node i. So for the k^{th} phase (where $k \in 1,...n$) we need to solve the LB equation (1), with k (possibly different) relaxation times. Values for various macroscopic variables in this model then follow almost analogously to the single phase equations for density, viscosity and momentum flux for each phase.

To model immiscibility between phases we implement the *pseudo-potential* model (Shan and Chen, 1993) which employs nearest neighbour inter-particle potentials to model the interactions between components. In a sense this follows physical reality at the microscopic level where molecules interact via short-range Lennard-Jones type potentials. In the original Shan-Chen model (Shan and Chen, 1993) lattice nodes which have a separation of less than or equal to $2^{1/2}$ units are coupled together. The interaction potential between components is accommodated via a force, F^k which is introduced through the added force term (Eq. (4)). The equilibrium velocity is re-defined to accommodate multiple phases, i.e., $\boldsymbol{u}_k^{eq} = \boldsymbol{u}'$. Here $\boldsymbol{u}'$ is a combined velocity and to satisfy momentum conservation must be

$$\boldsymbol{u}' = \frac{\sum_k \tau_k^{-1} \rho_k \boldsymbol{u}_k}{\sum_k \tau_k^{-1} \rho_k} \quad . \qquad (9)$$

The fluid-fluid interaction for phase k at lattice node $\boldsymbol{r}$ is then given by

$$\boldsymbol{F}^k(\boldsymbol{r}) = \rho_k(\boldsymbol{r}) c_s^2 \sum_{k \neq k'} g_{kk'} \sum_i w(|\boldsymbol{e}_i|^2) \times \rho_{k'}(\boldsymbol{r} + \boldsymbol{e}_i)\boldsymbol{e}_i \quad , \qquad (10)$$

where $g_{kk'}$ is the interaction potential (or coupling parameter) between dissimilar components. The weights w depend on the separation between interacting nodes with $w(1)$=1/6 and $w(2)$=1/12. Note, we assume the coupling is zero for similar components. The pressure in this model is given by the equation of state

$$P = c_s^2 \sum_k \rho_k + 3 \sum_{kk'} g_{kk} \rho_k \rho_{k'} \, . \qquad (11)$$

One of the issues with this nearest neighbour implementation is that it leads to large spurious currents which are a numerical artefact. These numerical artefacts, if not reduced to a minimum, will lead to large numerical instabilities. Thus we shall attempt to reduce these numerical instabilities. It has been found (Porter *et al*, 2012) extending the range of the pseudo-potential leads to a significant reduction (up to 1000 times) of these spurious currents. The range of pseudo-potential can in principal go to infinity but this of course comes at a computational cost. We have implemented here both 6th order (including all neighbours less than or equal to 2 units away) and 8th order (including all neighbours less than or equal to $8^{1/2}$ units away) pseudo-potentials. This increases the number of neighbours to be sampled from 18 (Shan-Chen) to 32 (6th order) to 64 (8th order), but greatly enhances the numerical stability of the method. Weights, which are required in Eq. (9), for the additional neighbour pairs have been given by Sbragaglia *et al* (2007).

The final step in the gray-scale, multiphase LB model is to incorporate the effect of voxel resistivity to flow. We assume the resistivity of a particular voxel can be different for different phases. Physically this may be the case if there are different materials in a voxel which have different slip conditions with different fluids. So equation (5) becomes:

$$f_i^k(\boldsymbol{r} + \boldsymbol{e}_i \Delta t, t + \Delta t) = (1 - n_s^k) f_i^k(\boldsymbol{r}, t) - \frac{1}{\tau_k}(1 - n_s^k) \times \left[f_i^k(\boldsymbol{r}, t) - f_i^{k,eq}(\boldsymbol{r}, t)\right] + (1 - n_s^k)\Im_i^k + n_s^k \hat{f}_i^k(\boldsymbol{r}, t). \quad (12)$$

The macroscopic velocity for each phase is defined similarly to equation (6) with suitable n_s^k, f^k and $\boldsymbol{F}^k$ values used for each component.

RESULTS

This multiphase LB model has previously been validated (Pereira, 2015) for a number of test cases (i.e., Laplace's law, contact angles, capillary pressure) as well as on packed beds and real porous media samples. Good agreement was found in test cases and the multiphase flows in packed beds and real porous media exhibited physically realistic characteristics. So here we concentrate on the gray-scale, multiphase model results.

For the simulations presented here we use $\tau_1 = 1$, $\tau_2 = 2.0$, which implies $\nu_1 = 1/6$, $\nu_2 = 1/2$, the mass of phase 1 is 1.0 while mass of phase 2 is 2.0. The surface tension g_{12} between phases is 4.0. Note, that unless we use the numerically stable multiphase model described above, we would not be able to have a disparity in these values (between the phases) and such a large g_{12} value.

Multiphase channel flow

We initially look at two-phase channel flow, i.e. phase 1 displacing phase 2 in a narrow channel (width 42 units, depth 22 units and length 152 units). We tried a range of n_s values to see how the flow changed. Figure 2 (which is a slice taken at the middle of the smallest dimension) shows flows for a variety of n_s values with a given body force. For the cases n_s = 0.05, 0.1, 0.3 and 0.5 we use a body force of 6.8×10^{-3} while for n_s = 0 if we use such a large body force the simulation is numerically unstable (i.e. too large speeds are generated). Thus for n_s = 0 the largest body force we can use (for a numerically stable simulation) is 6.8×10^{-4}. We also use a longer channel for n_s = 0 to accommodate higher speeds. For n_s = 0.7 a body force of 6.8×10^{-2} is applied.

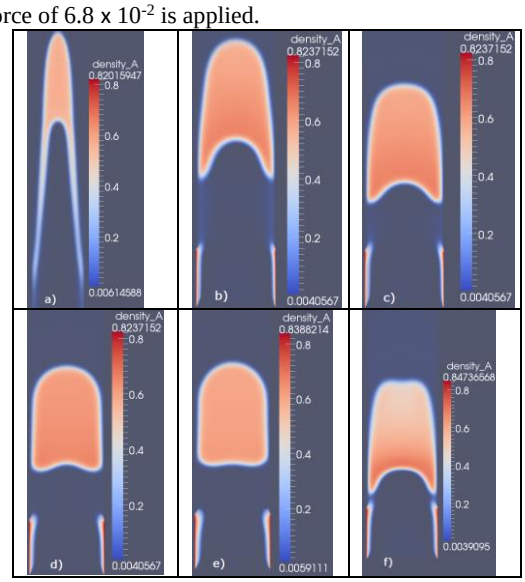

Figure 2: Two phase flow in a channel of width 41 units and depth 21 units for varying n_s. The A phase (orange hue) begins at the bottom of the channel (where the two orange stripes can be seen). a) For n_s = 0 and after 725 LB time steps, b) for n_s = 0.05 and after 1000 LB time steps, c) for n_s = 0.1 and after 2100 LB time steps, d) for n_s = 0.3 and after 13000 LB time steps and e) for n_s = 0.5 and after 50000 LB time steps, f) for n_s = 0.7 and after 19500 LB time steps.

The shape of the interfaces in Fig. 2 result from a combination of the surface tension, applied body force and applied n_s value. In Fig. 2a although the n_s value is zero, the comparatively large body force results in a large fluid velocity, which yields a highly curved (parabolic) interface profile. As the n_s value is increased, the interface becomes less curved and more flattened, in keeping with the results from Fig. 1. A larger body force needs to be applied as the n_s value is increased because n_s is directly related to fluid drag (Balsubramaniam et al, 1987, Dardis and McCloskey, 1998).

According to Darcy's Law the average velocity in a porous medium is given by

$$\langle V_x \rangle = \frac{Gk}{\nu\rho} \quad . \qquad (13)$$

So the average velocity is proportional to the permeability, k. In the gray-scale models (Walsh et al, 2009) the permeability is related to n_s via

$$k = \frac{(1-n_s)\nu}{2n_s} \quad , \qquad (14)$$

so that the average velocity along the channel is given by

$$\langle V_x \rangle = \frac{G(1-n_s)}{2n_s\rho} \quad . \qquad (15)$$

We can determine the average velocity quite easily in these simulations by tracking the location of the advancing interface (fluid front). Doing this for the four different simulations (at the same G value) and plotting the average velocity as a function of n_s gives Fig. 3. Note, we have also added the n_s = 1 value which gives zero channel speed (see equation (6)). We obtain a linear relationship between the average channel velocity and $(1\text{-}n_s)/n_s$, as predicted by equation (15). Furthermore, from the gradient of the graph and assuming an average A-phase density of 0.75, we predict the body force is 6.9×10^{-3}, which agrees well with the body force we have applied in these cases.

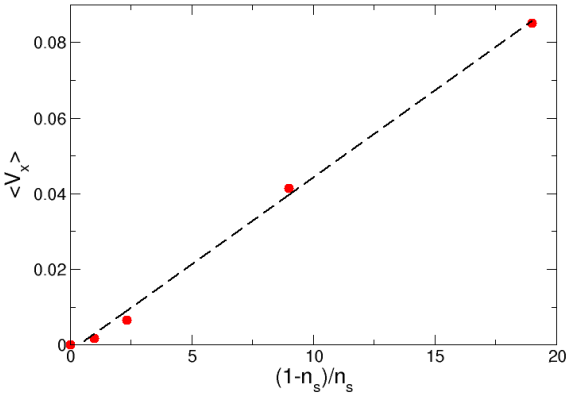

Figure 3: Plot of the average channel velocity of phase A versus $(1\text{-}n_s)/n_s$. Red circles come from LB simulations and dashed line is a best fit to these results (with gradient 4.6×10^{-3}).

Multiphase flow with n_s values which depend on phase

We now consider the physically interesting possibility of n_s values which vary depending on the phase which is present. This possibility is important because in certain materials, the slip velocity is certainly fluid dependent, i.e., a non-wetting fluid will have a different slip velocity to a wetting fluid. Thus a particular voxel may present different resistance to different fluids.

We therefore set up a multiphase channel flow simulation in a similar way to above. The only difference now is that

the n_s value corresponding to phase A is zero while the n_s value corresponding to phase B is 0.1. The time evolution for this case is shown in Fig. 4. Interestingly, two fingers develop in the channel. This is indicative of *viscous fingering*, which is a well-known physical phenomenon when a less viscous fluid displaces a more viscous fluid (Chen, 1987). It has previously been shown that the interface between the fluid phases is (mathematically) unstable to small sinusoidal perturbations (Paterson, 1981). It is quite significant that such a result naturally develops from this LB simulation. At the moment, this simulation becomes numerically unstable after 1000 LB times steps. A detailed study of this case is beyond the scope of the present work, but will be reported on in a future publication.

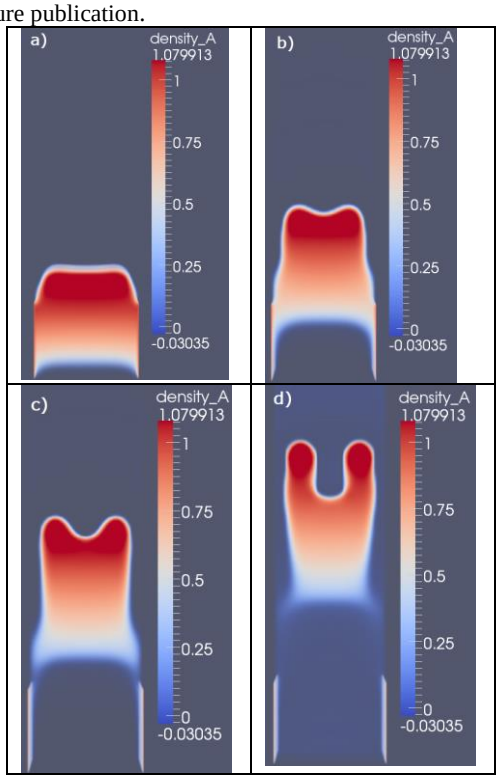

Figure 4: Evolution of channel flow in case where the n_s value depends on the phase present. We use n_s(A)=0.0, n_s(B)=0.1 a) Initially, b) after 300 LB time steps, c) after 600 LB time steps and d) after 1000 LB time steps.

Flow in the presence of semi-permeable objects

Given good agreement for channel flow between theory and our simulation we now proceed to some other important tests. We consider multiphase flow around cylindrical objects (tows) of higher n_s value compared to the bulk (Spaid and Phelan, 1998). In these simulations the domain is periodic in all directions, so we focus on the flow around and through the semi-permeable tows. There are five tows spaced equi-distantly apart (see white circles in Fig. 5a). These tows are given an n_s value of 0.07 for the A-phase and 0.0 for the B-phase. Everywhere else both phases are given an n_s value of 0.0.

Figure 5 shows the progress of the flood (from bottom to top) through and around the tows. As the flood proceeds the tows cause the flow to slow down (when the flow is through them). They also leave small voids in the tow regions which subsequently fill.

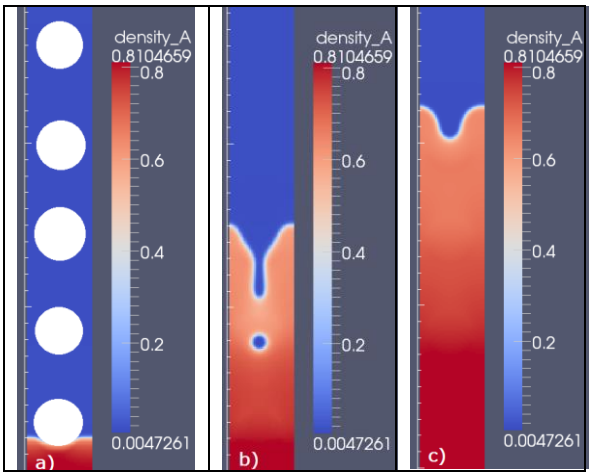

Figure 5: Evolution of flow through and around circular tows. a) Initially, b) after 3000 time steps and c) after 6000 times steps.

Spaid and Phelan (1998) have shown that the interface location, $\Re(t)$, (between phases) can be predicted from Darcy's Law as follows

$$\Re(t) = \frac{Gk}{\nu\rho\varepsilon} t \quad , \qquad (16)$$

where ε is the porosity (one minus the tow volume divided by total volume). We can track the interface position in this simulation and plot it as function of time (see Fig. 6a). (The interface between phases is calculated by finding the point where the largest gradient in the A phase density occurs along the vertical line which goes through the centre of all cylinders.) The black dots are the LB data and the red dashed line is a linear best fit to the data. The data follows a line reasonably well. However there are deviations due to (i) the initial transition to steady state conditions and (ii) oscillations in the profile as the interface reaches a tow (where it slows down) and then after it passes the tow (it speeds up).

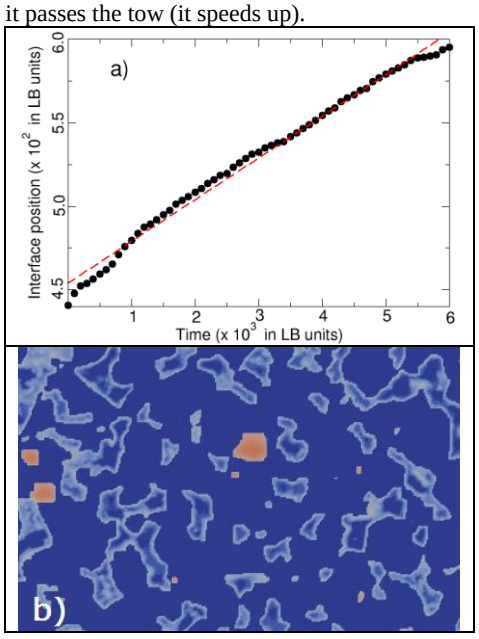

Figure 6: a) Plot of interface position versus time for the porous tow simulation shown in Fig. 5. b) Composition plot from a real CIPS sample (red denotes solid regions and blue represents void regions with a whitish hue in between these limits).

Multiphase flow for real samples

Finally we consider multiphase flow through real rock samples. These samples are from a CIPS (calcite *in situ* precipitation system) core sandstone sample which consists of calcite and quartz (Li et al, 2014b). The composition plot of this sample is shown in Fig. 6b. The sample is 200 x 200 x 5 LB units, with periodic boundary conditions in all directions. We consider a flood with the A-phase fluid reservoir at the left-hand edge of the sample, with the B-phase initially residing in the sample and a body force of 6.8 x 10^{-3} is applied in the positive *x*-direction. Figure 7 shows the progress of the flood at various time intervals.

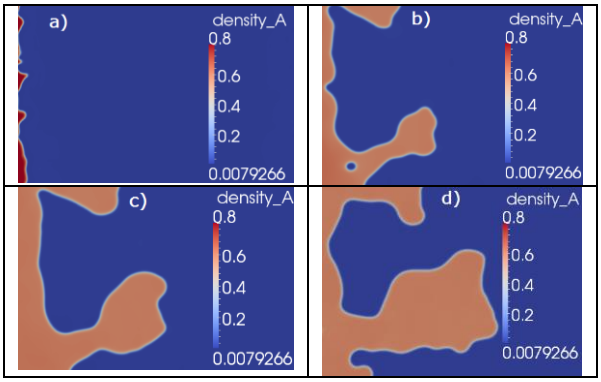

Figure 7: Progress of multiphase flood through a CIPS sample (whose composition is shown in Fig. 6b). a) Initial, b) after 10000 LB time steps, c) after 20000 LB time steps and d) after 40000 LB time steps.

In the composition map (Fig. 6b) for the CIPS sample one can see two small high composition regions close to the left edge. As a consequence soon after the flood begins (Fig. 7b) the middle region close to the left edge is bypassed and the flood begins with two main fingers along the top and bottom edges of the sample. These fingers grow as the flood proceeds. Another high composition region which is roughly in the middle of the sample prevents the two fingers from coalescing, which means a significant amount of the B-phase remains in the sample. This is typical of real oil floods, where fingering of the invading phase can lead to low overall yields.

CONCLUSION

In this study we have introduced a multiphase, gray-scale LB method which models multiphase fluid flow through semi-porous materials. The important quantity in this model is the fluid bounce-back fraction, n_s. This quantity can be defined for each voxel in the sample and also each phase in the sample and relates to the resistance to flow that a particular voxel presents to fluid.

We have applied the model to a few test cases (channel flow, flow around tows) and the agreement with theory is good. This gives us confidence in future applications of the model. We have also applied the model to cases where the n_s value depends on the fluid passing through. Here we observed something that was indicative of viscous fingering. This is a significant result and requires further investigation to understand completely. Finally, we applied the model to multiphase flow through a real rock (CIPS) sample. Here we observed that the invading phase bypassed regions of high composition. Although this is expected, it indicates the model is capable of correctly modelling multiphase fluid flow. In the future this model will be applied to bigger (fully three-dimensional) samples to determine real, multiphase relative permeability curves.

REFERENCES

BALASUBRAMANIAM, K., HAYOT, F. and SAAM, W.F., (1987) "Darcy's law from lattice- gas hydrodynamics", *Phys. Rev. A*, **36**, 2248–2253.

CHEN, S. and DOOLEN, G.D. (1998). "Lattice Boltzmann method for fluid flows". *Ann. Rev. Fluid Mech.*, **30**, 329-364.

CHEN, J.D., (1987), "Radial viscous fingering patterns in Hele-Shaw cells", *Exp. in Fluids*, **5**, 363-371.

DARDIS, O. and McCLOSKEY, J., (1998) "Lattice Boltzmann scheme with real numbered solid density for the simulation of flow in porous media", *Phys. Rev. E*, **57**, 4834–4837.

GAO, Y. and SHARMA, M.M., (1994) "A LGA model for fluid flow in heterogeneous porous media", *Transp. in Por. Media*, **17**, 1–17.

HE, X., CHEN, S. and DOOLEN, G. (1998). "A novel thermal model for the lattice Boltzmann method in the incompressible limit". *J. Comput. Phys*., **146**, 282 - 300.

LI, R.R., YANG, Y.S., PAN, J., PEREIRA, G.G., TAYLOR, J.A., CLENNELL, B. and ZOU, C., (2014a), "Lattice Boltzmann modelling of permeability in porous materials with partially percolating voxels", *Phys. Rev. E*, **90,** 033301(1-10).

LI, R.R, CHU, C., YANG, Y.S. and PEREIRA, G.G, CSIRO Data Access Portal (2014b), doi:10.4225/08/53F6E72A0D35E.

LIU, J., PEREIRA, G.G., and REGENAUER-LIEB, K., (2014), "From characterisation of pore-structures to simulations of pore-scale fluid flow and the upscaling of permeability using micro-tomography: A case study of heterogeneous carbonates", *J. Geochem. Expl*., **144**, 84-96.

PATERSON, L., (1981), "Radial fingering in a Hele-Shaw cell", *J. Fluid Mech*., **113**, 513-529.

PEREIRA, G.G., (2015), "Lattice Boltzmann simulations applied to understanding the stability of multiphase fluid interfaces", in "Progress in Applied CFD", *Sintef Academic Press, Oslo, Norway*, 231-237.

PORTER, M.L., E.T.COON, E.T., KANG, Q., MOULTON, J. and CAREY, J.W. (2012). "Multicomponent inter-particle potential lattice Boltzmann model for fluids with large viscosity ratios". *Phys. Rev. E*, **86**, 036701(1 - 8).

SBRAGAGLIA, M., BENZI, R., BIFERALE, L., SUCCI, S., SUGIYAMA, S. and TOSCHI, F. (2007). "Generalized lattice Boltzmann method with multirange pseudopotential". *Phys. Rev. E*, **75**, 026702(1 - 13).

SHAN, X. and CHEN, H. (1993), "Lattice Boltzmann model for simulating multiple phases and components". *Phys. Rev. E*, **47**, 1815 - 1819.

SPAID, M.A.A. and PHELAN, F.R., (1998), "Modelling void formation dynamics in fibrous porous media with the LB method", *Composites*, **29A**, 749-755.

SUCCI, S., (2001), "The Lattice Boltzmann Equation for fluid dynamics and beyond", *Oxford University Press, Oxford*.

WALSH, S.D.C., BURWINKLE, H., SAAR, M.O. (2009), "A new partial bounce-back LB method for fluid flow through heterogeneous media", *Comput. Geosci*., **35**, 1186-1193.